P H Y S I C A L   R E V I E W   L E T T E R S

Compressive Stress in Polycrystalline Volmer-Weber Films

R. Koch, Dongzhi Hu, and A. K. Das

Paul-Drude-Institut für Festkörperelektronik, Hausvogteiplatz 5-7, D-10117 Berlin, Germany

The Volmer-Weber mode for growing polycrystalline films, which comprises island, network, and channel stages before the films become continuous, is well known for its complex stress behavior with compressive and tensile stress alternating in the initial three growth stages. Recently, two new mechanisms for the compressive stress have been proposed [Phys. Rev. Lett. **88**, 156103 (2002); **89**, 126103 (2002)], which account for the reversibility of stress generation and relaxation. We show that the two mechanisms play only minor roles for the development of compressive stress, which is confirmed to be due to capillarity effects in the precoalescence stage.

The vast majority of thin films in technological applications are polycrystalline. A very common growth mode of polycrystalline thin films is the Volmer-Weber mode, which is well known to comprise three different growth stages: (i) the precoalescence stage, where isolated islands nucleate and grow, (ii) the coalescence stage, where islands merge and percolate and the remaining channels are filled, and (iii) the final stage, where henceforth a continuous film is growing. Previous investigations have shown that the evolution and relaxation of stress [1–4] during the Volmer-Weber growth of metals depend strongly on the surface mobility, leading to two types of characteristic thickness dependence of the stress irrespective of the materials (e.g., Ag [5–8], Cu [7,9–11], Au [9,10], Al [12], Fe [13], Cr [13], Ni [14], and Ti [15]). Figures 1(a) and 1(c) serve to illustrate these findings by means of two Fe films deposited at 310 and 520 K, respectively. At 310 K, where the surface mobility of Fe is low [13], a small compressive stress contribution is observed shortly after opening the shutter, i.e., in the precoalescence stage, whereas at higher film thickness the stress is tensile [Fig. 1(a)]. Upon interrupting deposition the stress remains nearly constant. Note that in Fig. 1 the film force F/w (with w denoting the width) is plotted, which depends linearly on thickness (t) for constant stress ($F/w = \sigma t$). At 520 K, i.e., at higher surface mobility, the overall stress behavior is more complex [Fig. 1(c)]. The film forces are slightly compressive in the precoalescence stage, tensile in the coalescence stage, and dominated again by a compressive stress contribution in the continuous film. Furthermore, when the deposition is stopped, a tensile stress component arises that saturates asymptotically with time.

Meanwhile, it is generally accepted that attractive forces along the grain boundaries give rise to tensile stress [16–20], which is the dominant stress mechanism in low mobility films. The compressive stress of the high mobility Volmer-Weber films, on the other hand, is still discussed controversially. Recently two mechanisms for the compressive stress in the precoalescence and postcoalescence stages of Volmer-Weber growth have been proposed, which were particularly motivated by the reversibility of stress

relaxation and generation observed during and after growth interruptions. As shown by Fig. 1(d) a large compressive force develops when growth at 520 K is resumed that gradually converges into a constant slope, similar to the one before the growth interruption. According to the model of Chason *et al.* [8], the postcoalescence compressive stress is associated with the flow of adatoms into nonequilibrium states of grain boundaries due to the flux-induced change of the surface chemical potential. When the deposition is stopped, atoms are moving out of the grain boundaries again, thereby relaxing compressive stress. Friesen *et al.* [11] observed the reversible compressive or tensile stress also in the precoalescence stage, i.e., in the absence of grain boundaries. They suggested that these stress changes are due to changes in the adatom population during and after deposition and inferred a similar scenario also for the postcoalescence regime.

According to a third stress model for Volmer-Weber growth by Abermann and co-workers [2,3], two different mechanisms are responsible for the compressive and tensile stress contributions, respectively. In this model the
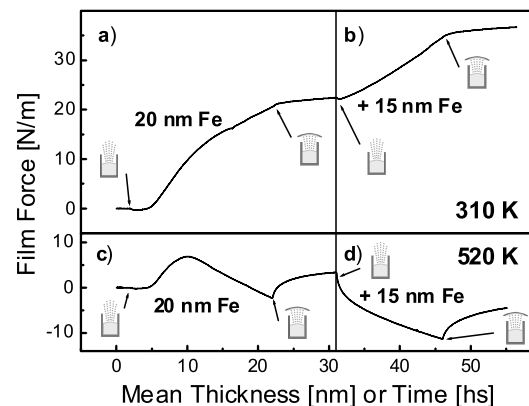

FIG. 1. Film forces (F/w) evolving during the deposition of 20 nm Fe onto oxidized Si(001) substrates at 310 K (a) and 520 K (c); after a growth interruption of 15 min an additional 15 nm layer was deposited at 310 K (b) and 520 K (d); tensile (compressive) stress is positive (negative).

compressive stress in the postcoalescence stage actually originates in compressive strain built up in the precoalescence stage [21]. Since the lattice spacing of isolated islands is smaller than in the bulk owing to a Laplace pressure (i.e., surface tension or stress) [22], a reduced lattice spacing is frozen-in at percolation [23]. Upon further growth the reduced lattice spacing, which corresponds to a nominal misfit of $\sim 0.1\%$, is propagated into the continuous film [21] (see Ref. [24]). The tensile stress observed during growth interruptions, on the other hand, is the result of ongoing recrystallization processes [25], as detected by *ex situ* transmission electron microscopy [26].

The goal of the present study is to find out which of the three models is actually representing the experiments: (A) compressive or tensile stress due to reversible movement of atoms in and out of the grain boundaries or (B) compressive or tensile stress due to surface chemical potential dependent change in adatom population, and (C) compressive stress resulting from capillarity effects in the precoalescence stage and tensile stress in growth interruptions due to recrystallization. From the experiments at hand, it is not possible to decide which of the three models is the appropriate one. For instance, the (almost) constant stress during growth interruptions at room temperature deposition of Fe [Fig. 1(b)] can be explained by negligible recrystallization (model C) or by a mobility that is too low for Fe atoms to be incorporated into grain boundaries (model A). Furthermore, the magnitude of compressive stress is determined by the number of grain boundaries ($\propto 1/d$) in model A and the island size at percolation ($\propto 1/d_p$) in model C; thus in both models, A and C, its magnitude is related inversely to the grain size. Therefore the increase of compressive stress with decreasing percolation thickness found in previous studies [13,27] is qualitatively consistent with both model A and model C. Also the experiment at different deposition rates described in Ref. [8] is not conclusive as no structural information is provided and it is well known that the Ag recrystallizes considerably even at room temperature [26]. The same argument holds for model B because Oswald ripening cannot be ruled out during growth interruptions in the precoalescence stage of Cu films; dissolving very small islands with high Laplace pressure in favor of larger ones reduces compressive stress, thus leading to a net tensile stress.

For our study we choose Fe as the film material. Compared to Ag and Cu employed in the studies discussed above, Fe behaves like a low mobility film at room temperature [cf. Fig. 1(a)] and a high mobility metal at 520 K [cf. Fig. 1(c)], thus providing more flexibility in selecting grain size and surface mobility as well as for conserving the morphology for structural investigation. The Fe films were prepared in a UHV chamber (base pressure $<2 \times 10^{-10}$ mbar) equipped with a sensitive cantilever beam device [28] and a scanning tunneling microscope (STM) for *in situ* stress measurements and structural investigations. The $25 \times 5 \times 0.15$ mm^3 Si(001) samples served as

cantilever beam substrates, which were cut with Si[100] parallel to the length. Prior to the Fe deposition, the substrates were degassed at 720 K for 30 min and then thermally equilibrated at the respective deposition temperature. Fe was electron beam evaporated from a Knudsen-type W crucible at a pressure of $(6–8) \times 10^{-10}$ mbar and a rate of 0.01 ± 0.002 nm/s as determined by a quartz crystal microbalance. The stress was evaluated by Stoney's formula [29] adapted to the geometry of our experimental setup. For calibration the substrate deflection due to its weight after rotation by 180° was measured. In each experimental run a cantilever beam and an STM substrate were prepared simultaneously to guarantee identical preparation conditions. Immediately after the film preparation, the STM sample was transferred to the STM chamber without breaking UHV and imaged at room temperature.

Before addressing the origin of compressive stress, we discuss the morphological evolution of low and high mobility Fe films. Figure 2 shows *in situ* STM images of the 310 and the 520 K films at thicknesses of 20 and 35 nm, corresponding to the growth interruptions in Fig. 1. As expected, the morphology of the 310 K film [Figs. 2(a) and 2(e)] is nearly independent of the film thickness. The average grain size $\bar{d}$ is almost constant with a value of ~ 7 nm at both thicknesses [30]. Therefore our STM investigations confirm previous findings [13] that Fe grows by columnar grains at 310 K owing to low atom mobility. $\bar{d}$ of the 520 K film, on the other hand, is considerably larger [Fig. 2(f)] and furthermore increases with thickness, e.g., from 10 to 17 nm when the film thickness is raised from 20 nm [Fig. 2(f)] to 35 nm [Fig. 2(g)], respectively. Obviously in higher mobility Fe films the grains also grow laterally, leading to a coarsening both during and after deposition. Note that recrystallization processes—leading to a change in the grain boundary density—are not included in models A and B. Only model C considers them as a possible source of stress.

In order to directly study the influence of the grain boundary density on the compressive stress, we prepared Fe films with different average grain sizes and used them as substrates for further Fe deposition. In all cases the deposition temperature for the subsequent Fe films was identical, namely, 520 K, to establish a constant Fe surface mobility. Figure 2(b) shows the morphology of a 20 nm thick Fe film which was deposited at 310 K, then heated to 520 K, and thermally equilibrated for 1 h to stabilize the cantilever beam device for the stress measurements. Compared with the unannealed 310 K film [Fig. 2(a)], the $\bar{d}$ has raised to 8.5 nm [Fig. 2(b)]. During the deposition of two additional 15 nm Fe layers, $\bar{d}$ increases further to 9.8 nm [Fig. 2(c)] and 13.0 nm [Fig. 2(d)], respectively. Figures 2(g) and 2(h) correspond to analogous experiments starting with a 20 nm Fe film deposited at 520 K. In that case $\bar{d}$ increases from originally 10.4 nm [Fig. 2(f)] to 17.2 nm [Fig. 2(g)] and 21.3 nm [Fig. 2(h)], respectively. $\bar{d}$ of the various films is summarized in Table I.
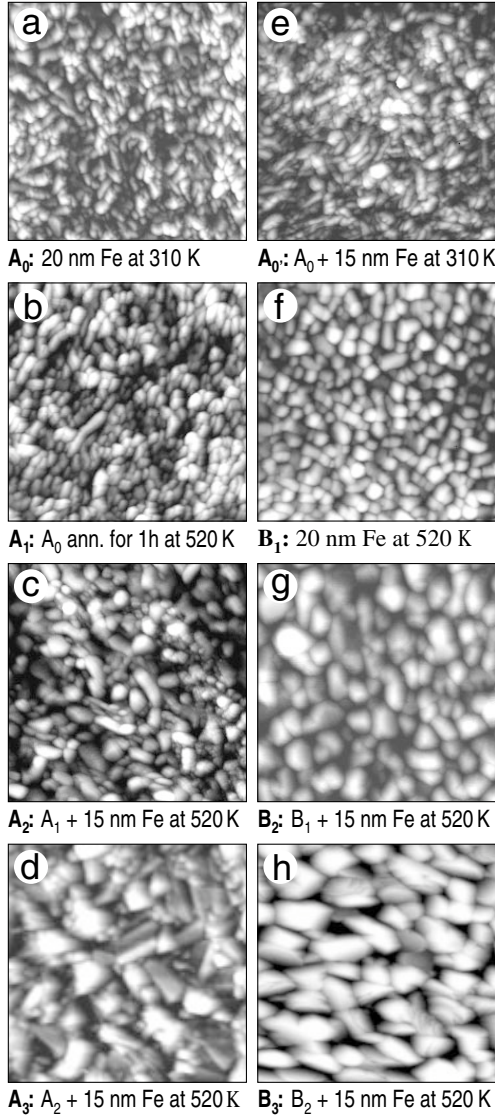
FIG. 2. The 180×180 nm^2 STM images of various Fe films: (a) 20 nm Fe deposited at 310 K onto the native oxide of Si(001) (A_0), (b) A_0 annealed for 1 h at 520 K (A_1), (c) A_1 + 15 nm Fe deposited at 520 K (A_2), (d) A_2 + 15 nm Fe deposited at 520 K (A_3), (e) A_0 + 15 nm Fe deposited at 310 K, (f) 20 nm Fe deposited at 520 K onto the native oxide of Si(001) (B_1), (g) B_1 + 15 nm Fe deposited at 520 K (B_2), and (h) B_2 + 15 nm Fe deposited at 520 K (B_3).

The force curves measured during deposition of the second and third Fe layers are shown in Fig. 3. On each substrate film the steady state stress σ_{ss}, i.e., the compressive stress calculated from the final slope of the force vs thickness curves, is nearly identical for the two additional Fe layers. On the other hand, the tensile force ΔF_t developing during the growth interruptions increases from the second to the third layer (cf. Table I). In view of the morphological results discussed above, the observed stress behavior is not consistent with a grain-size-related effect. As revealed by STM, the final grain size increases by $\sim 50\%$ compared with that of the 310 K substrate film

TABLE I. Average grain size $\overline{d}$ and steady state stress σ_{ss} developing during the deposition of various Fe films as well as the change in tensile force ΔF_t measured during growth interruptions.

Nr.	Deposition parameters	$\overline{d}$	σ_{ss} (GPa)	ΔF_t (N/m)
A_0	20 nm at 310 K	7.4	+0.77	+1.3
A_1	A_0 ann. for 1 h at 520 K	8.5		
A_2	A_1 + 15 nm at 520 K	9.8	−1.7	+5.6
A_3	A_2 + 15 nm at 520 K	13.0	−1.5	+7.9
B_1	20 nm at 520 K	10.4	−0.92	+5.9
B_2	B_1 + 15 nm at 520 K	17.2	−0.52	+6.6
B_3	B_2 + 15 nm at 520 K	21.3	−0.51	+7.8

and by $\sim 110\%$ in the case of the 520 K substrate film. Since in or out diffusion of atoms at grain boundaries according to model A depends inversely on $\overline{d}$, both σ_{ss} and ΔF_t should decrease significantly. Therefore model A can be clearly ruled out by our measurements.

Figure 4 compares the stress changes observed during growth interruptions in a continuous film with that in a discontinuous one. The measurements clearly show that the force changes in the continuous film are more than 1 order of magnitude larger. Moreover, ΔF_t increases decisively with film thickness (compare also Table I), whereas our STM data show that the local surface curvature, determining the adatom density via the step-step distance, remains nearly unchanged during grain coarsening. Particularly, our findings in the continuous film therefore are not consistent with model B.

Turning now to model C: Here σ_{ss} is determined by the island radius at percolation (R_p). Its magnitude can be estimated by the Laplace pressure as $\sigma_L = -2\gamma/R_p$ with γ being the surface tension. With $R_p = 3.7$ nm for the
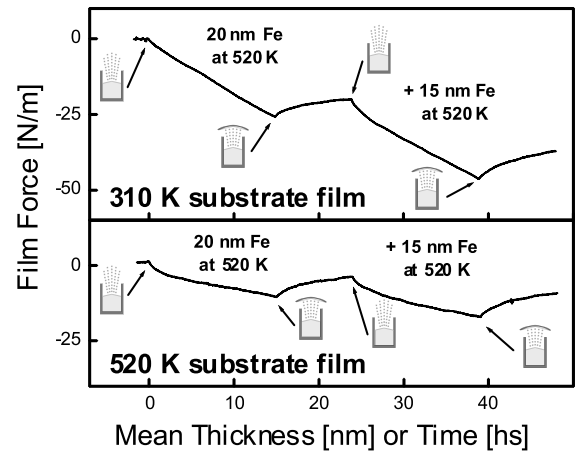

FIG. 3. Film forces (F/w) evolving during the subsequent deposition of two 15 nm Fe layers at 520 K onto 20 nm Fe substrate films deposited at 310 (top) and 520 K (bottom), before deposition of the second layer growth was interrupted for 15 min.
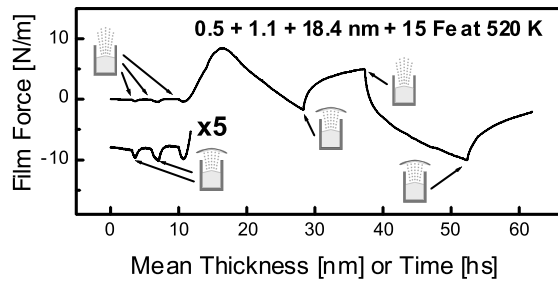
FIG. 4. Film forces (F/w) evolving during deposition of Fe onto an oxidized Si(001) substrate at 520 K; growth was interrupted after deposition of 0.5, 1.6, 20, and 35 nm.

310 K film, as suggested by Fig. 2(a), σ_L is -1.2 GPa ($\gamma_{310\,K} = 2.3$ J/m^2, extrapolated from the melting point value of Fe [31]). This value is in excellent agreement with the decrease in tensile stress observed in Fig. 1(a) at a thickness of about 8 nm (-1.3 GPa), where the 310 K film becomes continuous and the "Laplace stress" becomes effective. Raising the temperature to 520 K increases the equilibrium distance of Fe. Because of the different thermal expansion of Fe and Si, an additional compressive strain is introduced that increases the compressive stress during further growth by -0.4 GPa to a total value of -1.6 GPa. For the 520 K film we determine $R_p = 5$ nm from the thickness of tensile stress maximum in Fig. 1(b) ($\sim 2R_p$, see Ref. [10]) and obtain $\sigma_L = -0.88$ GPa ($\gamma_{520K} = 2.2$ J/m^2). Both σ_L values compare well with σ_{ss} of the films A$_2$ (-1.7 GPa) and B$_1$ (-0.92 GPa) which, however, includes also the tensile stress contributions of grain boundaries and recrystallization. According to model C, the magnitude of σ_{ss} decreases slightly with film thickness, when the strain information from the interface gets gradually lost due to the incorporation of defects.

In summary, our data show that (1) the steady state compressive stress is largely independent of grain size, and (2) the reversible tensile rise upon interruption of deposition increases with film thickness. Models A and B fail to explain the combination of these two effects, but neither observation is inconsistent with capillary effects being responsible for the compression. However, neither capillarity nor recrystallization can explain the reversible tensile rise itself. We speculate that postgrowth surface flattening, where material moves away from the compressive surface regions between grains and then reattaches in the tensile grain boundary regions, could lead to a rapid "tensile rise." When growth is resumed, the original surface configuration in recovered by initially accumulating impinging atoms preferentially at the compressively strained regions again. Since this process proceeds via surface diffusion, it is very fast in high mobility films. Furthermore, the magnitude of the effect will increase with grain size, as is observed. However, more work needs to be done to experimentally verify this model and to predict its magnitude.

[1] M. F. Doerner and W. D. Nix, CRC Crit. Rev. Solid State Mater. Sci. **14**, 225 (1988).
[2] R. Abermann, Vacuum **41**, 1279 (1990).
[3] R. Koch, J. Phys. Condens. Matter **6**, 9519 (1994).
[4] R. Koch, *The Chemical Physics of Solid Surfaces*, edited by D. A. King and D. P. Woodruff (Elsevier, Amsterdam 1997), Vol. 8, p. 448.
[5] R. Abermann and R. Koch, Thin Solid Films **66**, 217 (1980).
[6] R. Koch, D. Winau, A. Führmann, and K. H. Rieder, Phys. Rev. B **44**, 3369 (1991).
[7] A. L. Shull and F. Spaepen, J. Appl. Phys. **80**, 6243 (1996).
[8] E. Chason, B. W. Sheldon, L. B. Freund, J. A. Floro, and S. J. Hearne, Phys. Rev. Lett. **88**, 156103 (2002).
[9] R. Abermann and R. Koch, Thin Solid Films **129**, 71 (1985).
[10] D. Winau, R. Koch, A. Führmann, and K. H. Rieder, J. Appl. Phys. **70**, 3081 (1991).
[11] C. Friesen and C. V. Thompson, Phys. Rev. Lett. **89**, 126103 (2002).
[12] R. Abermann, Thin Solid Films **186**, 233 (1990).
[13] G. Thurner and R. Abermann, Thin Solid Films **192**, 277 (1990).
[14] D. Winau, R. Koch, and K. H. Rieder, Appl. Phys. Lett. **59**, 1072 (1991).
[15] M. Popeller and R. Abermann, Thin Solid Films **295**, 60 (1997).
[16] F. A. Doljack and R. W. Hoffman, Thin Solid Films **12**, 71 (1972).
[17] W. D. Nix and B. M. Clemens, J. Mater. Res. **14**, 3467 (1999).
[18] S. C. Seel, C. V. Thompson, S. J. Hearne, and J. A. Floro, J. Appl. Phys. **88**, 7079 (2000).
[19] L. B. Freund and E. Chason, J. Appl. Phys. **89**, 4866 (2001).
[20] J. A. Floro, S. J. Hearne, J. A. Hunter, P. Kotula, E. Chason, S. C. Seel, and B. W. Sheldon, J. Appl. Phys. **89**, 4886 (2001).
[21] R. Abermann, R. Koch, and R. Kramer, Thin Solid Films **58**, 365 (1979).
[22] C. W. Mays, J. S. Vermaak, and D. Kuhlmann-Wilsdorf, Surf. Sci. **12**, 134 (1968).
[23] R. Abermann, R. Kramer, and J. Mäser, Thin Solid Films **52**, 215 (1978).
[24] R. C. Cammarata, T. M. Trimble, and D. J. Srolovitz, J. Mater. Res. **15**, 2468 (2000).
[25] P. Chaudhari, J. Vac. Sci. Technol. **9**, 520 (1972).
[26] R. Koch and R. Abermann, Thin Solid Films **140**, 217 (1986).
[27] R. Abermann and R. Koch, Thin Solid Films **142**, 65 (1986).
[28] M. Weber, R. Koch, and K. H. Rieder, Phys. Rev. Lett. **73**, 1166 (1994).
[29] G. G. Stoney, Proc. R. Soc. London A **82**, 172 (1909).
[30] $\overline{d}$ was determined by hand from the grain density; similar values and the same trend are obtained from the grain area.
[31] N. Eustathopoulos, B. Drevet, and E. Ricci, J. Cryst. Growth **191**, 268 (1998).